

Regulated reconstruction of long-time spin–boson dynamics and emergent zero-bias transverse measurement primitive

Dragomir Davidovic^{1,*}

¹*School of Physics, Georgia Institute of Technology, USA*

(Dated:)

Time-convolutionless (TCL) master equations can break down at long times: time-local perturbative generators develop secular growth in correlation-dominated regimes. We mitigate this by a regulated, partially resummed reconstruction of the *dynamical map* around a Davies reference semi-group, expressed through a non-Markovian density-matrix correlator $\mathbf{C}(t)$ that remains bounded at late times. An exactly solvable rotating-wave benchmark links generator growth to interference-induced near-zeros of the coherence and shows how the reconstruction regulates the map. Applying the method to the unbiased spin–boson model reveals an emergent transverse measurement primitive: bath memory and counter-rotating terms induce phase lock-in that *irreversibly erases* the relative phase between σ_x eigenspaces on a finite timescale t_P , yielding an effective zero-bias transverse (σ_x) measurement channel. The selected transverse basis is not assumed *a priori*; it follows from the reconstructed reduced dynamics. The effect disappears in the rotating-wave approximation and in the Davies weak-coupling limit, demonstrating its non-Markovian interference origin.

I. INTRODUCTION

Understanding long-time open-system dynamics is central to quantum readout, noise modeling, and emerging measurements. In the decoherence/einselection viewpoint, preferred bases emerge as the states most stable under environmental monitoring [1–3]. At the same time, practical time-local descriptions such as time-convolutionless (TCL) master equations can break down at long times: perturbative generators develop secular growth and become ill behaved precisely in correlation-dominated regimes [4, 5]. In partially resummed TCL constructions this pathology can appear as an *exponential* late-time amplification of time-local rates; we refer to this specific form of secular growth as *secular inflation*. Here we address this TCL breakdown directly. Using the unbiased spin–boson model as a concrete testbed, we develop a regulated, partially resummed TCL reconstruction that remains controlled at late times and yields a controlled long-time reduced dynamics. Once this regime becomes accessible, the same analysis reveals an emergent *transverse measurement primitive*: the qubit phase-locks to the bath correlator and the reduced dynamics *erases* relative σ_x phase on a finite timescale t_P , producing an effective zero-bias σ_x measurement channel without positing a pointer basis *a priori*.

Previous analyses of einselection in the spin–boson model [1, 2] have primarily emphasized decoherence in the σ_z basis or polaronic pointer states in biased or ultrastrong-coupling regimes [6, 7]. These approaches capture environmental monitoring, but they do not yield an effective measurement channel in the unbiased model under factorized preparations and weak coupling.

In contrast, the mechanism identified here is interference-driven and depends on long-time memory

and counter-rotating physics; it is absent both in the rotating-wave approximation and in the Davies weak-coupling limit, where axial (σ_z) phase covariance enforces σ_x – σ_y symmetry and precludes transverse quadrature selection.

Measurement and amplification models typically specify the readout channel *a priori* via an effective detector Hamiltonian and an input–output description [8]. Here, we do not posit a detector model or pointer basis; instead we regulate the TCL long-time description and read off an effective measurement primitive operationally from the resulting reduced dynamics. We use the term *measurement primitive* in an operational, open-systems sense: a reduced completely positive, trace-preserving (CPTP) evolution that transfers information about an observable to inaccessible environmental degrees of freedom and thereby irreversibly suppresses the corresponding coherences. Concretely, for a transverse basis $\{\Pi_{\pm}\}$ with $\Pi_{\pm} = (1 \pm \sigma_x)/2$, the ideal nonselective projection is $\mathcal{M}_x(\rho) = \sum_{\pm} \Pi_{\pm} \rho \Pi_{\pm}$; our claim is that for $t \gtrsim t_P$ the reconstructed dynamics approximates this projection (up to finite contrast) even at zero bias. The resulting evolution is not quantum nondemolition (QND), since coherence magnitude flow can coexist with phase erasure. In this sense, the measurement interpretation is an outcome of the TCL analysis rather than an *a priori* measurement construction.

A key ingredient is long-time bath memory. Quantum decay generically deviates from a pure exponential at late times (the Khalfin effect) [9–11], and recent work proposes concrete observables to probe this post-exponential regime in open systems [12]. For slow bath correlations, algebraic tails can dominate and imprint their phase on the remaining coherence, motivating the phase-lock-in picture developed in Sec. IV.

A central technical obstacle is that time-local perturbative generators can develop secular growth and late-time instabilities, so that straightforward TCL truncations may become ill behaved precisely in the correlation-

* dragomir.davidovic@physics.gatech.edu

dominated regime. For algebraically decaying bath correlations, recent analyses of high-order TCL expansions make this breakdown explicit and quantify associated validity and precision limits [4]. Related progress on asymptotic higher-order generators for the spin–boson model further shows that increasing the TCL order can reshape inferred non–Markovianity in a regime-dependent way [13], reinforcing the need for controlled long-time descriptions. Complementary efforts have explored structural modifications intended to make TCL more resistant to breakdown, for example by replacing the required inverse with a Moore–Penrose pseudoinverse; in benchmark models this can tighten convergence conditions and reduce accuracy, with terms that scale unfavorably with bath dimension [5]. Similar late-time secular growth appears beyond TCL, e.g., in open-system effective field theory treatments of Unruh–DeWitt detectors, where resummation is required for reliable late-time predictions [14], while a complementary line of work restores physicality at the dynamical-map level via Choi–proximity regularization, projecting an approximate non–Markovian map to the nearest CPTP evolution [15].

Against this background, we analyze the dynamics using partially resummed TCL expansions, building on standard TCL constructions for non–Markovian open quantum systems [16, Chap. 9]. The scalar correlator $C(t)$ is promoted to a matrix-valued *density-matrix correlator* $\mathbf{C}(t)$, and the generator is regularized by resumming the dominant secular structures around an appropriate reference semigroup. The resulting dynamical map interpolates between the weak-coupling (Lindblad) regime and the correlation-driven long-time limit, yielding an explicit long-time readout-channel description.

The present work makes two contributions. First, we mitigate late-time secular growth by developing a regulated, partially resummed reconstruction of the dynamical map that stays controlled in the correlation-dominated regime. Second, once this late-time regime becomes accessible, the same reconstruction uncovers an emergent measurement primitive in a minimal microscopic setting: non–Markovian memory and counter-rotating terms generate an effective zero-bias transverse (σ_x) measurement primitive in the unbiased spin–boson model. In this sense the measurement interpretation is an outcome of the TCL analysis rather than an *a priori* measurement model, and the effect is absent both in the rotating–wave approximation and in the Davies weak–coupling limit.

The remainder of the paper develops the regulated TCL framework and applies it to the unbiased spin–boson model. Sections II and III introduce the theoretical construction and the regularization ansatz. Section IV presents the Khalfin–Peres picture of non-exponential decay and the resulting phase lock-in. Section V benchmarks the method on an exactly solvable rotating–wave model. Section VI analyzes the full spin–boson dynamics and the resulting late-time quadrature selection, while Sec. VII presents the numerical results. Section VIII dis-

cusses broader implications and applications, followed by conclusions.

II. THE STANDARD OPEN SYSTEM SETUP

We consider a finite–level system weakly coupled to a bosonic bath, with total Hamiltonian

$$H_T = H_S + H_B + H_I. \quad (1)$$

The self–Hamiltonian is diagonal in its energy basis,

$$H_S = \sum_{n=1}^N E_n |n\rangle\langle n|, \quad (2)$$

with Bohr frequencies $\omega_{nm} = E_n - E_m$. The bath is a collection of harmonic modes,

$$H_B = \sum_k \omega_k b_k^\dagger b_k, \quad (3)$$

and the system–bath coupling is taken in separable form

$$H_I = A \otimes F, \quad (4)$$

where A is a Hermitian system operator and

$$F = \sum_k g_k (b_k + b_k^\dagger) \quad (5)$$

is a Hermitian bath operator with $g_k \propto \lambda \ll 1$.

In the interaction picture the reduced dynamics are governed by the bath correlation function

$$C_\beta(t) = \langle F(t)F(0) \rangle_\beta, \quad (6)$$

defined with respect to a thermal state at inverse temperature β . We characterize the bath by the spectral density

$$J_\omega = \pi \sum_k g_k^2 \delta(\omega - \omega_k), \quad (7)$$

so that

$$C_\beta(t) = \frac{1}{\pi} \int_{-\infty}^{\infty} d\omega J_{\beta,\omega} e^{-i\omega t}, \quad J_{\beta,\omega} = \frac{J_\omega}{1 - e^{-\beta\omega}}. \quad (8)$$

We use the phenomenological form

$$J_\omega = 2\pi\lambda^2 \frac{\omega^s}{\omega_c^{s-1}} e^{-\omega/\omega_c} \Theta(\omega), \quad (9)$$

with cutoff ω_c and spectral exponent s (Ohmic $s = 1$, sub–Ohmic $0 < s < 1$, super–Ohmic $s > 1$). At $T = 0$ this yields

$$C(t) = \frac{2\lambda^2 \Gamma(s+1)}{(1 + i\omega_c t)^{s+1}}. \quad (10)$$

A convenient quantity is the half-sided transform

$$\Gamma_{\beta,\omega} = \int_0^\infty dt C_\beta(t) e^{i\omega t} = J_{\beta,\omega} + iS_{\beta,\omega}, \quad (11)$$

which is analytic for $\text{Im } \omega > 0$. Its finite-time counterpart

$$\Gamma_{\beta,\omega}(t) = \int_0^t d\tau C_\beta(\tau) e^{i\omega\tau} \quad (12)$$

is entire in ω and approaches $\Gamma_{\beta,\omega}$ as $t \rightarrow \infty$.

III. PARTIALLY RESUMMED TCL AND MAP RECONSTRUCTION

We now specify the partially resummed TCL generator $L(t)$ used below and the corresponding map-level reconstruction for $\mathbf{C}(t)$. Following Ref. [4], we employ a closed-form partial resummation of the leading secular cumulants of the TCL generator, yielding a master equation

$$L(t) = -i[H_S, \cdot] + K(t), \quad (13)$$

with dissipator

$$\begin{aligned} K_{nm,ij}(t) = & A_{ni}A_{jm} \left[\Gamma_{\beta,\omega_{in}^{(j)}(t)}(t) + \Gamma_{\beta,\omega_{jm}^{(i)}(t)}^*(t) \right] \\ & - \sum_k \left[\delta_{jm}A_{nk}A_{ki}\Gamma_{\beta,\omega_{ik}^{(j)}(t)}(t) \right. \\ & \left. + \delta_{ni}A_{jk}A_{km}\Gamma_{\beta,\omega_{jk}^{(i)}(t)}^*(t) \right], \end{aligned} \quad (14)$$

where the renormalized complex frequencies are

$$\begin{aligned} \omega_{in}^{(j)}(t) = & \omega_{in} - i \left[\sum_c \left(|A_{ic}|^2 \Gamma_{\omega_{ic}}(t) - |A_{nc}|^2 \Gamma_{\omega_{nc}}(t) \right) \right. \\ & \left. + 2J_{\beta,0}(t) A_{jj} (A_{nn} - A_{ii}) \right]. \end{aligned} \quad (15)$$

The first term is the Fermi–Golden–Rule contribution, while the second is a spectral–overlap correction that couples populations and coherences beyond Born–Markov theory. The resummation captures the dominant late-time secular structures, but the generator breaks down once the renormalized frequencies cross into the lower half-plane, producing secular inflation [4].

Regulating this inflation is a central aim of the present work. We write the dynamical map as

$$\rho(t) = [e^{L_0 t} + \mathbf{C}(t)]\rho(0), \quad (16)$$

where $e^{L_0 t}$ is the Davies semigroup [17] and $\mathbf{C}(t)$ collects all non–Markovian corrections. The choice of $e^{L_0 t}$ as a reference flow is supported by the rigorous van Hove (weak-coupling) limit, in which the Davies semigroup

gives the exact reduced dynamics on the rescaled time $\tau = t\lambda^2$:

$$\lim_{\lambda \rightarrow 0} \|\rho_{\text{exact}}(\tau/\lambda^2) - e^{L_0 \tau/\lambda^2} \rho(0)\| = 0 \quad (\tau \text{ fixed}). \quad (17)$$

Thus $\mathbf{C}(t)$ naturally collects correlation-dominated corrections beyond the van Hove scaling regime. Additional support comes from rigorous weak-coupling strategies that treat an effective dissipative dynamics as the leading (“zero-order”) term [18] and from uniform-in-time Markovian approximation results [19].

In contrast to the Davies semigroup, time-local TCL partial resummations do develop negative effective rates and secular inflation in the generator at late times in correlation-dominated regimes. Differentiating Eq. (23) and using the inverse map gives the exact equation

$$\frac{d\rho}{dt} = [L_0 + \dot{\mathbf{C}}(t)e^{-L_0 t}] [1 + \mathbf{C}(t)e^{-L_0 t}]^{-1} \rho(t). \quad (18)$$

Within the Davies regime, the inverse admits a controlled expansion, exposing the secularly inflating structure,

$$\frac{d\rho}{dt} = \left[L_0 + (\dot{\mathbf{C}}(t) - L_0 \mathbf{C}(t))e^{-L_0 t} + \dots \right] \rho(t). \quad (19)$$

Matching to the partially resummed TCL generator $L(t) = L_0 + K^{(2)}(t) + K^{(4)}(t) + \dots$ yields the simple *ansatz*:

$$\dot{\mathbf{C}}(t) - L_0 \mathbf{C}(t) = [L(t) - L_0] e^{L_0 t}, \quad (20)$$

with solution

$$\mathbf{C}(t) = \int_0^t d\tau e^{L_0(t-\tau)} [L(\tau) - L_0] e^{L_0 \tau}. \quad (21)$$

This balances the secularly inflating TCL generator against the contractive Davies flow and yields a bounded $\mathbf{C}(t)$ as long as the Davies reference captures the leading dissipative scaling and the residual corrections remain subleading.

IV. INTERFERENCE EFFECTS AND PHASE LOCK-IN

For physical intuition behind the Davies reference flow and the correlator correction $\mathbf{C}(t)$, we recall the Khalfin–Peres picture of long-time decay, which separates a leading Markovian contribution from a correlation-controlled feedback term that dominates at late times.

A. Khalfin–Peres decomposition at long times

Khalfin first showed that nonstationary quantum states can deviate from exponential decay at late times due to dispersion effects [9]. Peres later recast this behavior using a finite “box” whose continuum limit is

taken as the volume $\rightarrow \infty$ [10]. In that representation the “environment” is the complementary subspace of the full Hilbert space, and the survival amplitude $f(t) \equiv \langle \psi(0) | \psi(t) \rangle$ admits the approximate decomposition

$$f(t) = e^{-(\gamma+i\omega)t} + \eta C(t), \quad (22)$$

where $C(t) = \langle \psi(0) | V(t) V(0) | \psi(0) \rangle$ is an environmental autocorrelation function of an effective interaction operator V acting on the complementary subspace. The first term captures the Markovian exponential contribution, while the second encodes delayed environmental feedback and typically decays algebraically. At intermediate times the exponential term dominates, whereas at late times the interference with $\eta C(t)$ governs the decay and produces the crossover to correlation-dominated relaxation.

If $C(t) \sim t^{-(s+1)} e^{i\phi}$ with $s > 0$, the algebraic tail ultimately overtakes the exponential in Eq. (22), and the survival amplitude phase-locks to $C(t)$:

$$f(t) \sim \eta t^{-(s+1)} e^{i\phi}, \quad t \rightarrow \infty.$$

In this regime the phase of $f(t)$ is set by the environment, while the envelope follows the power law $t^{-(s+1)}$. The resulting lock-in is measurement-like in the sense that a quadrature becomes asymptotically selected, but it is not a von Neumann measurement: it produces no stochastic outcomes or classical record, and it does not, by itself, erase relative phase information—it deterministically imprints the bath phase onto the surviving coherence (an explicit reduced-state example is given in the RWA benchmark in Sec. V).

B. From survival amplitudes to density matrices

To lift the same long-time interference structure to density matrices, we recall the map decomposition

$$\rho(t) = [e^{L_0 t} + \mathbf{C}(t)] \rho(0), \quad (23)$$

where $e^{L_0 t}$ is the Davies semigroup [17] and $\mathbf{C}(t)$ collects non-Markovian corrections. The regulated, partially resummed TCL construction developed in Sec. III then determines $\mathbf{C}(t)$ and makes the late-time interference physics accessible at the level of the full reduced state.

V. BENCHMARKING THE ANSATZ: ROTATING-WAVE APPROXIMATION

The rotating-wave approximation (RWA) provides an exactly solvable benchmark for our reconstruction scheme. Because both exact and TCL-based master equations are available in this limit [20, 21], the RWA cleanly exposes the origin of secular inflation and tests how the ansatz regulates it. The RWA provides an exactly solvable realization of the long-time interference picture introduced in Sec. IV.

A. RWA model and exact reduced dynamics

We consider the unbiased two-level system

$$H = H_S + H_B + H_I, \quad H_S = \frac{\Delta}{2} \sigma_z, \quad H_I = \frac{1}{2} \sigma_x \otimes F. \quad (24)$$

In the rotating-wave approximation we retain only number-conserving terms,

$$H_I \approx \frac{1}{2} (\sigma_+ \otimes F_- + \sigma_- \otimes F_+), \quad (25)$$

$$F_+ = \sum_k g_k b_k^\dagger, \quad F_- = \sum_k g_k^* b_k, \quad (26)$$

so that the total excitation number $N = \sigma_+ \sigma_- + \sum_k b_k^\dagger b_k$ is conserved. At $T = 0$ the dynamics from a single-excitation preparation is therefore confined to the $N = 1$ sector.

For an initial superposition

$$|\Psi(0)\rangle = c_1 |1\rangle + c_2 |2\rangle, \quad |c_1|^2 + |c_2|^2 = 1, \quad (27)$$

the exact reduced state has the form [21]

$$\rho_{\text{exact}}(t) = \begin{bmatrix} |c_1 f(t)|^2 & c_1 c_2^* f(t) \\ c_1^* c_2 f^*(t) & 1 - |c_1 f(t)|^2 \end{bmatrix}, \quad (28)$$

so all reduced dynamics is determined by the survival amplitude $f(t)$. In particular, the coherence evolves as $\rho_{12}(t) = f(t) \rho_{12}(0)$ and $\rho_{21}(t) = f^*(t) \rho_{21}(0)$. Equivalently, the transverse Bloch component satisfies

$$x(t) + iy(t) = 2\rho_{12}(t) = f(t) [x(0) + iy(0)].$$

Rotations about σ_z therefore commute with the reduced dynamics, and the evolution contracts/rotates the (x, y) plane isotropically. Hence the RWA benchmark cannot generate transverse quadrature selection.

In the interaction picture, $f'(t) = e^{-i\Delta t} f(t)$ obeys the exact Volterra equation

$$\dot{f}'(t) = -\frac{1}{4} \int_0^t d\tau C(t-\tau) e^{i\Delta(t-\tau)} f'(\tau), \quad (29)$$

which is the Peres survival-amplitude equation [10]. The explicit solution can be written as [21]

$$f(t) = \frac{1}{4\pi} \int_0^\infty d\omega \frac{e^{-i\omega t} J(\omega)}{[\Delta - \omega + S(\omega)/4]^2 + [J(\omega)/4]^2}. \quad (30)$$

Representative exact solutions for several spectral exponents are shown in Fig. 1. The coherence magnitude $|f(t)|$ crosses over from an initial exponential regime to a late-time algebraic tail, while the coherence phase locks to the bath correlation function after the phase lock-in time t_P , given by Eq. 34.

B. Pole-plus-tail interference and phase lock-in

The exact RWA expression (30) admits a transparent long-time interpretation in the interference picture

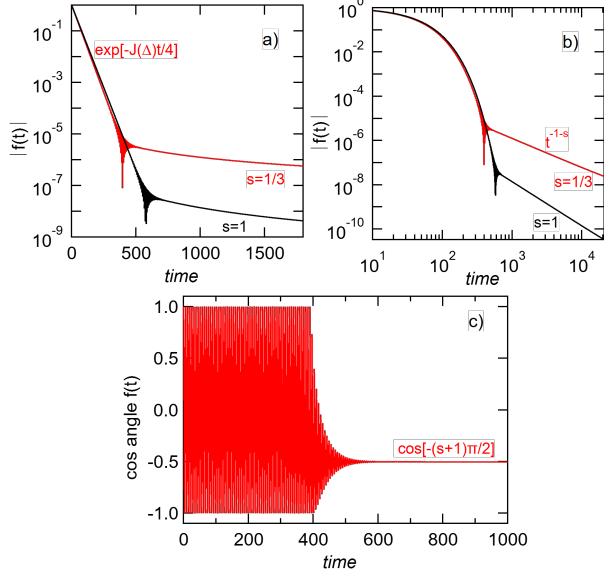


FIG. 1. Representative examples of long-timescale dynamics. (a,b) The amplitude $|f(t)|$ versus time on log-linear and log-log scales, illustrating the crossover from Markovian (exponential) to non-Markovian (power-law) decay. (c) Cosine of the coherence angle, showing the transition from oscillations at the system frequency around the z -axis to alignment with the bath correlation function, which eventually fixes the phase of the decaying coherence amplitude. In the vicinity of the phase lock-in time t_P , the amplitude exhibits interference-induced oscillations. Black: Ohmic bath with $s = 1$, $\lambda^2 = 0.025$; Red: sub-Ohmic bath with $s = 1/3$, $\lambda^2 = 0.01$; in both cases $\omega_c = 4$ and $\Delta = 1$.

of Sec. IV: it is well captured by the sum of a Markovian (pole) contribution and a correlator-controlled (tail) contribution, whose crossover produces phase lock-in and the precursor of secular inflation.

In the weak-coupling regime the integrand in Eq. (30) is sharply peaked near $\tilde{\Delta} = \Delta + S(\Delta)/4$. Expanding about this peak yields a Lorentzian lineshape and the Markovian exponential contribution

$$f_M(t) = e^{-[i\tilde{\Delta} + J(\Delta)/4]t}, \quad (31)$$

which accurately describes the coherence for $t \lesssim t_P$.

At late times, the dominant frequencies scale as $\omega \sim 1/t$, and the lineshape in Eq. (30) is controlled by its low-frequency behavior. Approximating the denominator by its $\omega = 0$ value gives the tail

$$f_C(t) \approx \frac{1}{4[\Delta + S(0)/4]^2} C(t), \quad (32)$$

which captures the algebraic decay for $t \gtrsim t_P$.

The exact coherence is therefore well approximated by the two-component form

$$f(t) \approx f_M(t) + f_C(t), \quad (33)$$

equivalent to the Khalfin–Peres decomposition. The phase lock-in time is defined by the balance condition

$$|f_M(t_P)| = |f_C(t_P)|, \quad (34)$$

which in weak coupling yields

$$t_P = (s + 1) T_2 \ln(\omega_c T_2). \quad (35)$$

Near t_P , interference between f_M and f_C produces narrow modulation windows in $|f(t)|$, ranging from transient bursts to near-extinctions and accompanied by near- π phase slips at destructive interference [Fig. 3(a,b)].

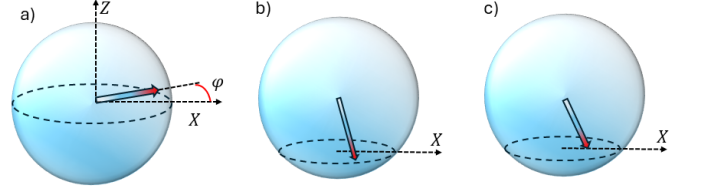


FIG. 2. Geometry of phase lock-in in the rotating-wave approximation (RWA) and its promotion to projective readout in the full spin–boson model. (a) Initial Bloch vector in the xy plane at azimuthal angle ϕ . (b) RWA: phase lock-in halts the precession while retaining x – y coherence; the transverse direction is shifted to $\phi - \pi(s + 1)/2$ and decays as $\sim t^{-s-1}$. (c) Full model: counter-rotating terms complete the projection into the xz plane, erasing x –basis residual coherence; the surviving transverse component again decays as $\sim t^{-s-1}$.

A central feature of the post–crossover regime is phase lock-in: for $t \gg t_P$ the phase of $f(t)$ becomes trapped to the phase of $C(t)$, suppressing the visibility of free precession. In the RWA the post–crossover dynamics falls short of a von Neumann measurement: the reduced state (28) preserves the information in c_1 and c_2 , with the bath imprinting a deterministic phase shift rather than erasing relative phase. Genuine projection onto the interaction axis requires counter-rotating terms (cf. Fig. 2).

We now connect these interference windows to the behavior of time-local generators. The exact RWA time-local generator extracted from Eq. (28) is

$$L_{\text{exact}}(t) = \begin{bmatrix} \frac{f}{f^*} + \frac{f^*}{f} & 0 & 0 & 0 \\ 0 & \frac{f^*}{f} & 0 & 0 \\ 0 & 0 & \frac{f}{f^*} & 0 \\ -\frac{f}{f^*} - \frac{f^*}{f} & 0 & 0 & 0 \end{bmatrix}, \quad (36)$$

in the ordering $(\rho_{11}, \rho_{21}, \rho_{12}, \rho_{22})$. Because $L_{\text{exact}}(t)$ contains ratios such as f/f^* , destructive interference can drive $f(t)$ close to zero and produce large generator spikes. As shown in Fig. 3(c), this yields inflation-like peaks clustered around t_P , followed by suppression at later times. This nonperturbative inflation arises directly from interference with $C(t)$ and serves as the microscopic origin of secular growth in time-local TCL generators.

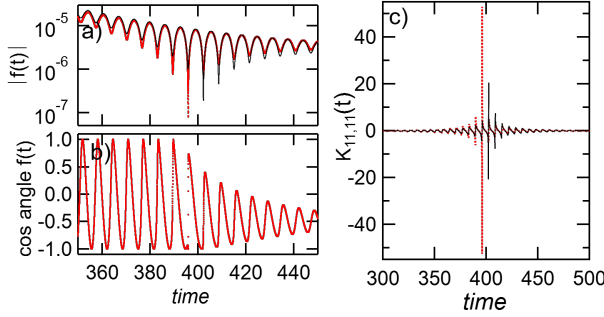


FIG. 3. Coherence magnitude (a), phase (b), and population generator (c) near t_P . Constructive interference produces bursts; destructive interference leads to near-extinctions with a near- π phase slip at $t_P = 396$. Generator inflation (c) appears in the exact dynamics, showing spikes up to 10^3 above rate $1/T_1$, recurring at Δ' . Red dotted: exact solution; black solid: two-component interference model. Parameters: $s = 1/3$, $\lambda^2 = 0.01$, $\omega_c = 4$, $\Delta = 1$.

C. Reconstructing the Exact Dynamics Beyond TCL Breakdown

To connect the exact RWA dynamics to perturbative TCL resummations, we build the time-local coherence generator from the van Kampen cumulant expansion of the Volterra equation (29). For algebraically decaying bath correlators, cumulants beyond a critical order $n_{\max}(s)$ regain secular growth [4], so the cumulant series itself requires partial resummation. A leading resummation produces a self-consistent complex frequency shift, Eq. (37), which yields the inflated TCL generator used below. The full cumulant construction, its secular classification via the Δ identity, and the emergence of nested renormalizations are given in Appendix X.

1. Partial resummation results

The leading resummation yields a renormalized frequency

$$u = \omega - \frac{i}{4}\Gamma_\omega(t), \quad (37)$$

so that the resummed generator takes the form

$$\left. \frac{\dot{f}'}{f'} \right|_{\text{resum}} = -\frac{1}{4}\Gamma_u(t) + O(\lambda^4). \quad (38)$$

Subleading and nested corrections are discussed in Appendix X.; they do not modify the main conclusions in the parameter regime of interest.

The Schrödinger-picture partially resummed generator follows from Eq. (36) by replacing f/f with its resummed

counterpart, yielding

$$L(t) = \begin{bmatrix} -\frac{1}{2}\text{Re}\Gamma_u(t) & 0 & 0 & 0 \\ 0 & i\Delta - \frac{1}{4}\Gamma_u^*(t) & 0 & 0 \\ 0 & 0 & -i\Delta - \frac{1}{4}\Gamma_u(t) & 0 \\ \frac{1}{2}\text{Re}\Gamma_u(t) & 0 & 0 & 0 \end{bmatrix}, \quad (39)$$

which exhibits secular inflation beyond t_P .

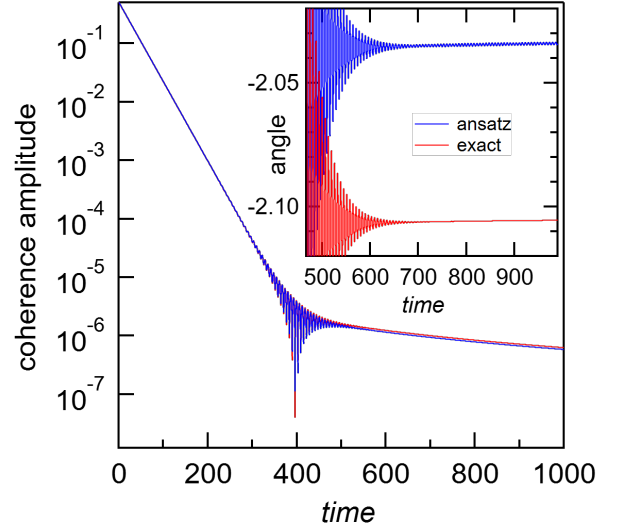


FIG. 4. **Coherence dynamics: exact vs reconstructed solutions.** The partially resummed coherence reproduces the exact dynamics in both amplitude and phase, including the late-time regime around $t \sim t_P$, demonstrating the efficacy of the ansatz. Parameters: $s = 1/3$, $\lambda^2 = 0.01$, $\omega_c = 4$, $\Delta = 1$, $T = 0$, $t_P = 396$.

For the RWA Hamiltonian the Davies generator is

$$L_0 = \begin{bmatrix} -\frac{1}{2}J_\Delta & 0 & 0 & 0 \\ 0 & i\tilde{\Delta} - \frac{1}{4}J_\Delta & 0 & 0 \\ 0 & 0 & -i\tilde{\Delta} - \frac{1}{4}J_\Delta & 0 \\ \frac{1}{2}J_\Delta & 0 & 0 & 0 \end{bmatrix}. \quad (40)$$

Since $[L(t), L_0] = 0$, the correlator ansatz reduces to

$$\mathbf{C}(t) = e^{L_0 t} \int_0^t d\tau [L(\tau) - L_0]. \quad (41)$$

In the long-time limit this yields a coherence-sector correlator

$$[\mathbf{C}(t)]_{12,12} = -\frac{1}{4}\Sigma_{-\tilde{\Delta}+i\nu_2}(t), \quad (42)$$

with

$$\Sigma_\omega(t) = \int_0^t d\tau \tau C(t-\tau) e^{i\omega\tau}. \quad (43)$$

For $t \gg T_2$ the integral is dominated by $\tau \lesssim T_2$, so that $\Sigma_\omega(t) \approx -\omega^{-2}C(t)$ and Eq. (42) reduces to the late-time tail in Eq. (32).

Figure 4 shows that the regulated reconstruction reproduces the exact coherence amplitude and phase across the full crossover, including the interference window near t_P . Thus, secular inflation in the early-time resummed generator already encodes the information needed to reconstruct the late-time coherence dynamics.

D. From the RWA to the Full Spin–Boson Model

The RWA benchmark shows how long-time bath memory can steer the dynamics toward a stable transverse quadrature, with phase lock-in and an algebraic coherence tail. However, the RWA omits counter-rotating processes and therefore cannot capture the full late-time geometry of the Bloch dynamics. We now turn to the full spin–boson model to quantify how number-conserving and nonconserving channels combine, and to assess the robustness of quadrature selection across bath exponents s and weak bias. The next section begins from the Markovian baseline and then analyzes the correlation-dominated regime where the long-time structure emerges.

VI. SPIN–BOSON MODEL (SBM)

The two-level system is now coupled to the environment as

$$H = H_S + H_B + H_I, \quad H_S = \frac{\Delta}{2} \sigma_z, \quad H_I = A \otimes F, \quad (44)$$

with

$$A = \frac{1}{2}(\xi \sigma_z + \sigma_x), \quad (45)$$

where ξ denotes the *bias parameter* and F is the bath operator introduced in Eq. 5.

The full dynamics of the unbiased or weakly biased spin–boson model is not known in closed form, even in the scaling limit [6]. As a starting point, and to establish notation, we begin with the standard Davies (Born–Markov) semigroup. This provides a controlled Markovian reference against which the correlated late-time behavior of interest can be contrasted.

A. Davies Semigroup Baseline

Within the Davies framework, all dynamical quantities exhibit purely exponential relaxation. The corresponding generator takes the form

$$L_0 = \begin{bmatrix} -J_{\beta,\Delta}/2 & 0 & 0 & J_{\beta,-\Delta}/2 \\ 0 & -\nu_{\beta,2} + i\tilde{\Delta} & 0 & 0 \\ 0 & 0 & -\nu_{\beta,2} - i\tilde{\Delta} & 0 \\ J_{\beta,\Delta}/2 & 0 & 0 & -J_{\beta,-\Delta}/2 \end{bmatrix}, \quad (46)$$

in the vectorization order $(\rho_{11}, \rho_{21}, \rho_{12}, \rho_{22})$. The Lamb-shifted frequency is $\tilde{\Delta} = \Delta + \frac{1}{4}(S_{\beta,\Delta} - S_{\beta,-\Delta})$.

Equation (46) is phase-covariant: the coherences ρ_{21} and ρ_{12} decay with the same rate $\nu_{\beta,2}$ and acquire opposite phases $\pm\tilde{\Delta}$, implying isotropic contraction and rotation in the transverse plane. Writing $x = \rho_{12} + \rho_{21}$ and $y = i(\rho_{21} - \rho_{12})$ yields $\dot{x} = -\nu_{\beta,2}x - \tilde{\Delta}y$ and $\dot{y} = -\nu_{\beta,2}y + \tilde{\Delta}x$, so σ_x and σ_y are treated equivalently and no transverse quadrature selection (i.e., no transverse measurement primitive) can emerge in the Davies limit.

Both populations and coherences decay exponentially with rates

$$\nu_{\beta,1} = \frac{1}{2}(J_{\beta,\Delta} + J_{\beta,-\Delta}) = \frac{1}{2}J_{\Delta} \coth \frac{\beta\Delta}{2}, \quad (47)$$

$$\nu_{\beta,2} = \frac{1}{4}(J_{\beta,\Delta} + J_{\beta,-\Delta}) + \xi^2 J_{\beta,0}, \quad (48)$$

and the decoherence time satisfies $T_2 = 2T_1$ at zero bias.

This Davies generator will serve as the contractive reference flow in the map decomposition (23), with $\mathbf{C}(t)$ capturing corrections outside the van Hove (weak-coupling) regime.

1. Competing Coherent and Environmental Dynamics

We consider an initial superposition,

$$\rho(0) = \frac{1}{2} \begin{bmatrix} 1 & e^{-i\phi} \\ e^{i\phi} & 1 \end{bmatrix}, \quad (49)$$

which places the Bloch vector in the xy plane at azimuthal angle ϕ . Assuming $\xi = 0$ or $T = 0$, decoherence is governed purely by relaxation.

Two interactions compete: (i) the Hamiltonian drives coherent precession about σ_z ; (ii) the coupling $(\sigma_x/2)F$ causes relaxation and entanglement with the bath when viewed in the σ_x basis. The Davies semigroup therefore cannot generate transverse quadrature selection: its phase covariance treats σ_x and σ_y equivalently (as shown above), so no preferred transverse axis can emerge within the van Hove validity window in Eq. (17).

At longer physical times and/or stronger effective coupling than the van Hove scaling assumes, bath memory breaks transverse phase covariance. In the correlation-dominated regime, interference with the long-time tail of the bath correlator drives phase lock-in and produces a transverse *measurement primitive*: on a finite timescale t_P the evolution erases the relative phase between σ_x eigenspaces and contracts the transverse Bloch vector toward a preferred σ_x quadrature (with weak contrast at the times studied). This is not a QND measurement of σ_x : although the azimuthal angle is pinned, $\langle \sigma_x \rangle$ continues to relax (toward zero), so the σ_x populations are not conserved.

2. Non-Markovian Semigroups

Alternative reference semigroups can be generated from asymptotic TCL2 or TCL4 generators [22, 23]. Although we do not use them here to cancel secular inflation, their stationary state coincides [to $\mathcal{O}(\lambda^2)$] with the reduced mean-force (Hamiltonian-of-mean-force) Gibbs state [24].

At $T = 0$ they yield

$$\rho_\infty = \begin{bmatrix} 0 & 0 \\ 0 & 1 \end{bmatrix} + \frac{1}{4} \begin{bmatrix} -\frac{\partial S}{\partial \omega} & 2\xi \frac{S(0) - S(-\Delta)}{\Delta} \\ 2\xi \frac{S(0) - S(-\Delta)}{\Delta} & \frac{\partial S}{\partial \omega} \end{bmatrix} \quad (50)$$

valid to $\mathcal{O}(\lambda^2)$, giving the leading Hamiltonian-of-mean-force corrections to the uncoupled Gibbs state $\rho_S^G \propto e^{-\beta H_S}$ (here $\beta \rightarrow \infty$).

B. Asymptotic analysis of $\mathbf{C}(t)$

Having fixed the Born–Markov (Davies) baseline, we now use the regulated TCL *map reconstruction* to access the correlated late-time regime. In this regime the dynamics no longer reduces to a fixed semigroup and straightforward time-local generators can exhibit secular inflation. By working at the level of the reconstructed dynamical map, encoded through the correlator $\mathbf{C}(t)$, we can characterize the late-time limit directly and determine which dynamical structures survive once long-time bath memory becomes important.

To confirm convergence and determine the resulting late-time map, we evaluate the asymptotic limit of $\mathbf{C}(t)$. We decompose $\mathbf{C}(t)$ into four dynamical sectors by introducing the projection superoperators

$$Q = \text{diag}(0, 1, 1, 0), \quad P = 1 - Q,$$

which isolate the coherence and population subspaces, respectively. From Eq. (46), the Davies generator commutes with both projectors, *i.e.*, $[L_0, Q] = [L_0, P] = 0$.

1. Population channels

We first consider the population channels $\mathbf{C}(t)P$, which govern relaxation and equilibration of the diagonal density-matrix components.

At finite temperature, the present ansatz does not fully regularize the population channels, and residual secular growth may reappear at parametrically late times. In the low-temperature regime $k_B T \ll \Delta$ relevant here, these contributions remain negligible up to $t \sim T_2(\Delta/k_B T)$. We therefore focus on the $T = 0$ population asymptotics, and defer a complete finite-temperature treatment to future work.

As a representative example, consider population-to-coherence transfer. The relevant subblock is

$$Q \mathbf{C}(t) P = \begin{bmatrix} \mathbf{C}_{21,11} & \mathbf{C}_{21,22} \\ \mathbf{C}_{12,11} & \mathbf{C}_{12,22} \end{bmatrix}.$$

Applying Q and P to Eq. (21) yields

$$Q \mathbf{C}(t) P = \int_0^t d\tau e^{L_0(t-\tau)} Q L P e^{L_0\tau}. \quad (51)$$

To isolate the asymptotic regime, we evaluate the superoperator products in the eigenbasis and perform the analytic integrations in the long-time limit, assuming that all renormalized frequencies have reached their asymptotic values. We retain only contributions that decay more slowly than $e^{-n\nu_2 t}$ (integer $n \geq 1$), since faster terms relax on the Davies timescale and do not influence the non-Markovian late-time map. These rapidly decaying contributions are important during the early Markovian stage and are included in the numerical integration, but they do not affect the asymptotic form.

The resulting convergence is

$$Q \mathbf{C}(t) P \xrightarrow{e^{-\nu_2 t} \ll 1} \frac{\xi}{2} \frac{S(0) - S(-\Delta)}{\Delta} \begin{bmatrix} 0 & 0 & 0 & 0 \\ 1 & 0 & 0 & 1 \\ 1 & 0 & 0 & 1 \\ 0 & 0 & 0 & 0 \end{bmatrix} + \mathcal{O}(\lambda^4). \quad (52)$$

Thus, the asymptotic population-to-coherence block reproduces the mean-force Gibbs coherences of Eq. (50), up to $\mathcal{O}(\lambda^4)$.

Next we examine the diagonal population sector $P \mathbf{C}(t) P$. The analysis proceeds similarly, and we obtain

$$P \mathbf{C}(t) P \xrightarrow{e^{-\nu_2 t} \ll 1} \frac{1}{4} \frac{\partial S}{\partial \omega} \begin{bmatrix} 1 & 0 & 0 & 1 \\ 0 & 0 & 0 & 0 \\ 0 & 0 & 0 & 0 \\ -1 & 0 & 0 & -1 \end{bmatrix} + \mathcal{O}(\lambda^4), \quad (53)$$

which reproduces the $\mathcal{O}(\lambda^2)$ corrections to the asymptotic populations in Eq. (50). Altogether, the population–channel asymptotics confirm that the ansatz generates corrections to the Davies map that are accurate through $\mathcal{O}(\lambda^2)$.

2. Coherence channels

We now turn to the coherence channels $\mathbf{C}(t)Q$, using the same asymptotic criterion.

The coherence-to-population sector $P \mathbf{C}(t) Q$ decays exponentially to zero as $t \rightarrow \infty$ for all temperatures, biases, and spectral exponents $s > 0$. The corresponding decay rate is bounded below by ν_2 , and we can safely neglect this block asymptotically.

The remaining coherence subblock,

$$Q \mathbf{C}(t) Q \equiv \begin{bmatrix} \mathbf{C}_{21,21} & \mathbf{C}_{21,12} \\ \mathbf{C}_{12,21} & \mathbf{C}_{12,12} \end{bmatrix} \xrightarrow{e^{-\nu_2 t} \ll 1} \frac{1}{4} \begin{bmatrix} -\Sigma_{\beta, -\tilde{\Delta} + i\nu_2 + iJ_{\beta,0}\xi^2}^*(t) & Z_{\beta, \tilde{\Delta}, \nu_2 + J_{\beta,0}\xi^2}(t) \\ Z_{\beta, \tilde{\Delta}, \nu_2 + J_{\beta,0}\xi^2}(t) & -\Sigma_{\beta, -\tilde{\Delta} + i\nu_2 + iJ_{\beta,0}\xi^2}(t) \end{bmatrix}, \quad (54)$$

arises from cancellations between exponentially growing and decaying terms, uncovering new long-time coherence dynamics. Here

$$\Sigma_{\beta, \omega}(t) = e^{-\frac{2\nu_2 t}{e^{\beta \tilde{\Delta}} - 1}} \int_0^t d\tau \tau C_{\beta}(t - \tau) e^{i\omega\tau}, \quad (55)$$

$$Z_{\beta, \Delta, k}(t) = e^{-\frac{2\nu_2 t}{e^{\beta \tilde{\Delta}} - 1}} \int_0^t d\tau \frac{\sin(\Delta\tau)}{\Delta} C_{\beta}(t - \tau) e^{-k\tau}. \quad (56)$$

A detailed analysis of Eqs. (55)–(56) shows that

$$\lim_{t \rightarrow \infty} Q \mathbf{C}(t) Q = 0$$

for arbitrary temperature, small bias, and any spectral exponent $s > 0$ within the weak-coupling regime where the regulated TCL construction is valid.

In the present weak-coupling formulation, the late-time coherence dynamics is governed by $\Sigma(t)$ and $Z(t)$, which encode the number-conserving and counter-rotating contributions, respectively. The RWA retains only the diagonal correlator $\Sigma(t)$ [cf. Eq. (42)] by neglecting the counter-rotating terms. Repeating the analysis following Eq. (43), we find that at late times the correlators become approximately equal in magnitude but opposite in sign:

$$\Sigma_{\beta, \omega}(t) \approx -Z_{\beta, \Delta, k}(t) \approx -e^{-\frac{2\nu_2 t}{e^{\beta \tilde{\Delta}} - 1}} \frac{C_{\beta}(t)}{\omega^2}, \quad t \gg 1/\nu_2. \quad (57)$$

Physically, the late-time behavior follows from how the regulated map reconstruction retains both the number-conserving and counter-rotating sectors in the coherence block. Away from the van Hove (Davies) scaling limit, their interference breaks transverse phase covariance and reshapes the coherence map: one transverse quadrature is suppressed while the other survives through phase lock-in to the bath correlation function. In other words, once the long-time map becomes accessible in a controlled way, the reduced dynamics itself implements a preferred transverse axis without imposing one by hand.

Mathematically, this appears as an emergent *measurement primitive* in the coherence sector. For $t \gtrsim t_P$, the action of $Q \mathbf{C}(t) Q$ on an initial state becomes approximately one-dimensional in the transverse plane: it maps a generic initial transverse coherence to its σ_x component and thereby erases the relative transverse phase (with weak contrast at the times studied). Concretely,

$$Q \mathbf{C}(t) Q \rho(0) \xrightarrow{t \gtrsim t_P} 2 \operatorname{Re}[Z_{\beta, \Delta, k}^*(t) \rho_{21}(0)] \sigma_x + \mathcal{O}(\Sigma_{\beta, \omega}(t) + Z_{\beta, \Delta, k}(t)), \quad (58)$$

which aligns the transverse Bloch vector with the interaction operator σ_x and suppresses the orthogonal quadrature. Unlike the RWA, this is not merely a passive phase shift of a preserved initial coherence; it is *finite-time phase erasure by dynamical alignment*, i.e., a nonselective transverse measurement primitive generated by the correlation-dominated map.

Importantly, the selected axis is not posited via a detector model or a predictability-sieve assumption; it follows from the structure of the spin–boson coherence map once the long-time interference terms are retained. The interaction singles out the σ_x quadrature in the correlation-dominated regime, while the orthogonal component cannot participate in the same lock-in mechanism. Consequently, $\langle \sigma_y \rangle$ continues to decay at the decoherence rate until a parametrically later time, set by the fact that Σ and Z are only approximately (not exactly) equal in magnitude and opposite in sign. This small imbalance is resolved explicitly in the numerical analysis of the next section.

3. Geometric picture of the dynamical projection

To make the projection mechanism explicit, we analyze the unbiased spin–boson model at $T = 0$ for the initial transverse superposition 49. The population component σ_z relaxes first at rate ν_1 , while the transverse component precesses at the renormalized frequency $\tilde{\Delta}$ and decays exponentially at rate ν_2 . At the lock-in time t_P , the σ_x component phase-locks to the bath correlation function and Eq. 58 reduces to

$$\cos \phi \sigma_x + \sin \phi \sigma_y \xrightarrow{t \gtrsim t_P} t^{-(s+1)} \cos \left[\phi - \frac{(s+1)\pi}{2} \right] \sigma_x. \quad (59)$$

Equation (59) expresses the transverse measurement primitive in a compact form: the transverse spin is driven toward the σ_x quadrature while the orthogonal quadrature is suppressed, and the surviving component crosses over to the universal algebraic tail $t^{-(s+1)}$ with a bath-induced phase shift. This should be contrasted with an ideal nonselective Lüders dephasing $\mathcal{M}_x(\rho) = \sum_{\pm} \Pi_{\pm} \rho \Pi_{\pm}$, which removes σ_x -relative phase without imposing the strong contraction present here. The contrast is therefore weak at the times studied: the dynamics produces phase erasure together with substantial attenuation of the surviving transverse component.

Once confined to the xz plane, the transverse amplitude decays algebraically and ultimately vanishes, so this is not a QND measurement of σ_x : although the azimuthal angle is pinned after t_P , $\langle \sigma_x \rangle$ continues to relax (toward zero) and the σ_x populations are not conserved. This “dynamical localization” is generated by long-time memory and occurs for any $s > 0$, in contrast to the true localization transition of the strong-coupling Ohmic model, which appears only for $s \leq 1$ [6]. The numerical results below visualize this gradual projection and confirm the analytic late-time behavior.

VII. NUMERICAL STUDIES

We illustrate the preceding regulated TCL *map reconstruction* with numerical simulations of the late-time dynamics at zero and weak bias while varying the bath exponent s . The goal is twofold: (i) to validate the reconstructed long-time map in regimes where time-local generators can exhibit secular inflation, and (ii) to visualize the dynamical crossover at t_P and the resulting transverse *measurement primitive* (finite-time phase erasure with weak contrast at the times studied). The same reconstruction can be applied to finite temperatures and to multilevel or multicoherence settings, providing a general route to controlled long-time reduced dynamics.

All results in this section are obtained by directly integrating Eq. 20 using a standard fourth-order Runge-Kutta scheme. This time-domain integration involves no asymptotic expansions or late-time approximations.

In the analytical discussion above we did not distinguish between the bare transverse Pauli operators and the quadratures that actually undergo phase locking, corresponding to the formal limit $\lambda \rightarrow 0$. In the numerical examples below we incorporate the small, environment-induced quadrature shift by an implicit rotation in the xy -plane,

$$\sigma_x \mapsto \cos \delta\phi \sigma_x + \sin \delta\phi \sigma_y, \quad (60)$$

$$\sigma_y \mapsto -\sin \delta\phi \sigma_x + \cos \delta\phi \sigma_y, \quad (61)$$

with a rotation angle $\delta\phi = O(\lambda^2)$ that scales linearly with the coupling. For notational simplicity we continue to denote the rotated operators by σ_x and σ_y ; thus, throughout this section, σ_x should be understood as the effective locking quadrature and σ_y as its orthogonal partner. The values of $\delta\phi$ used in each example are stated explicitly, and the procedure for extracting them from the dynamics is described in Appendix XI.

A. Emergent transverse measurement primitive in the unbiased spin-boson model

We now examine phase locking in the unbiased SBM using the parameters of Fig. 1. The qubit is initialized at zero temperature in the xy -superposition

$$\rho(0) = \frac{1}{2}(\mathbf{1} + \cos \phi \sigma_x + \sin \phi \sigma_y), \quad (62)$$

where ϕ is the transverse preparation angle defined under the implicit xy -plane rotation given above. As stated above, σ_x and σ_y already denote the rotated quadratures, and for this unbiased Ohmic example we incorporate the environment-induced alignment shift $\delta\phi = -0.0278$.

The Ohmic numerical results are shown in Fig. 5(a). Populations relax exponentially into the mean-force Gibbs state [Eq. (49)], independent of the preparation angle ϕ . The coherence exhibits an extended exponential regime followed by a sharp late-time crossover, closely

matching the lock-in transition observed for the RWA benchmark in Fig. 1. The delayed lock-in near $\phi \approx \pi/2$ shows strong resistance to transverse phase erasure when the initial quadrature is nearly orthogonal to the effective interaction axis. Although the locked coherence amplitude is small in this example (deliberately weak coupling), the basin geometry and ϕ -resolved crossover structure are already fully formed at late times.

The data in Fig. 5(a) deliberately use weak Ohmic coupling, for which the transverse measurement primitive has weak contrast and the crossover occurs only after many free-precession periods. As shown in Appendix XII, increasing λ^2 shortens t_P while leaving the late-time basin topology essentially unchanged. In this sense the same correlation-driven mechanism can be tuned toward a higher-contrast, faster transverse measurement primitive as the coupling is enhanced.

This tunability suggests a practical connection to engineered readout protocols: one can aim to *temporarily* increase the effective transverse coupling during a short readout window, thereby reducing t_P and increasing the contrast of transverse phase erasure. In circuit or cavity settings this could be emulated by driven, σ_x -polarized coupling or reservoir shaping that enhances the effective transverse noise seen by the qubit. We do not model such control fields here; we note it only as a route for translating the intrinsic spin-boson mechanism into a faster, higher-contrast readout channel.

Having established that the mechanism persists at larger coupling, we now return to the deliberately weak-coupling regime used above. This setting provides a magnified view of the dynamics, allowing the detailed structure of the projection—its angular dependence, interference windows, and basin organization—to be resolved by varying the system parameters.

B. Dependence on the Preparation Angle

To illustrate the basic features of the emergent transverse measurement primitive in the Ohmic case, Fig. 5(b) summarizes the dependence of the coherence lock-in time on the preparation angle ϕ across several bath exponents s . The approximate condition $\phi_{\text{peak}} \approx \pi(n - s/2)$ reflects the combined effect of the initial azimuthal phase and the bath-induced phase shift accumulated during lock-in. As the spectral exponent s varies, the memory kernel acquires a different phase response, shifting the location of maximal system-bath interference. The peak in t_P therefore marks angles where the transverse spin is nearly orthogonal to the effective interaction axis and most strongly resists projection.

Figures 5(c) and (d) show the family of coherence decay curves as ϕ sweeps $[0, \pi]$, and then zoom into the narrow region where t_P reaches its maximum. Shifting ϕ by π reproduces the same patterns, including the branching structure near the peak in Fig. 5(c). These behaviors stand in sharp contrast to the RWA model, which ex-

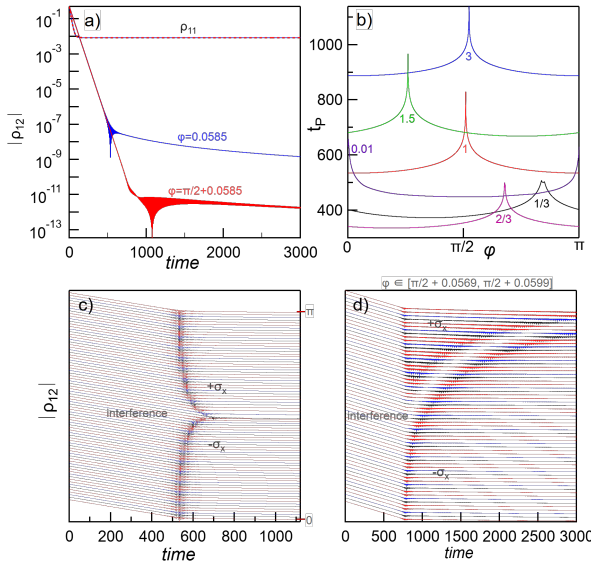


FIG. 5. Spin-boson dynamics in an Ohmic bath versus state preparation. (a) Populations and coherences versus time for $\phi = 0.0585$ (blue) and $\phi = \frac{\pi}{2} + 0.0585$ (red dashed); the two upper curves coincide. (b) Phase lock-in time t_P versus ϕ , extracted as the intercept between the early exponential decay ($t < t_P$) and the late power-law tail ($t > t_P$). Different bath exponents s are plotted, indicated beneath their respective peaks; the maxima occur near $\pi(n - s/2)$. (c) Coherence magnitude versus time for $s = 1$ and $\phi \in [0, \pi]$ in eighty increments, plotted on a logarithmic scale; curves are vertically offset for clarity. The right-hand ticks denote the endpoints of the angular sweep. $\phi = 0$ (lower) and $\phi = \pi$ (upper). (d) Same as (c), but zoomed into the narrow interval near $\pi/2$, revealing three disconnected regions separated by strong bath-induced quantum interference. Parameters: $s = 0.01, 1/2, 2/3, 1, 3/2, 3$ for $\lambda^2 = 0.005, 0.01, 0.02, 0.025, 0.05, 0.5$, respectively; other parameters $\omega_c = 4$, $\Delta = 1$, $\xi = 0$, $T = 0$.

hibits no dependence on ϕ .

The three disconnected regions in Fig. 5(c,d), separated by a band of strong interference, signal nontrivial late-time correlations when the transverse spin is nearly orthogonal to the interaction axis. In this case the transverse component is not simply extinguished; it partially resists projection, producing a more intricate landscape than a naive extinction picture would suggest. The dynamics is therefore not analogous to an optical setup with a perfectly perpendicular polarizer and analyzer, which would yield complete extinction.

This disconnected structure appears when the initial angle lies just around ϕ_{peak} . Strong bath interference then generates a sequence of dynamical regimes that cannot be captured by a single “orthogonal quadrature” picture. The pattern reflects two dynamical attractor basins in the unbiased spin-boson model, corresponding to late-time states with $\langle \sigma_x \rangle > 0$ and $\langle \sigma_x \rangle < 0$. The transverse spin undergoes a form of *dynamical localization* into these

basins: its direction becomes locked while its magnitude decays algebraically with the bath correlation function.

For initial angles slightly above ϕ_{peak} , the spin first locks into the basin with $\langle \sigma_x \rangle < 0$, then reenters an interference-dominated window where projection temporarily fails, and finally locks into the opposite basin with $\langle \sigma_x \rangle > 0$. The basins are therefore separated by narrow intervals—either in initial angle or in time—in which the projection mechanism is inefficient. As a result, three distinct late-time regions emerge instead of the two regimes expected from simpler models.

This should not be confused with Leggett’s localization transition, which is an equilibrium suppression of tunneling in the unbiased Ohmic model. Here the effect is dynamical: it arises from late-time interference under factorized system preparation, whereas Leggett localization relies on a polaronic initial state that effectively biases the system toward localization from the outset.

As we show next, this behavior depends strongly on the spectral exponent s , which clarifies the physical origin of the branching and the locations of the interference windows. Before turning to this s dependence, we first examine the time-resolved collapse to clarify the meaning of each of the three regions in Fig. 5(d).

C. Dynamics of the Collapse

To visualize the projective quantum evolution of the transverse spin component, we vary the initial azimuthal angle ϕ and compute the expectation values

$$\langle \sigma_x(t, \phi) \rangle = \text{tr}[\rho_\phi(t) \sigma_x], \quad \langle \sigma_y(t, \phi) \rangle = \text{tr}[\rho_\phi(t) \sigma_y],$$

where $\rho_\phi(t)$ denotes the time-evolved density matrix corresponding to the initial state specified in Eq. 62.

Figure 6 displays $\langle \sigma_x(\phi, t) \rangle$ and $\langle \sigma_y(\phi, t) \rangle$ as functions of the preparation angle ϕ at several times. During the initial Markovian stage of the evolution, the two quadratures decay nearly equally, while the phase precesses uniformly with angular frequency $\tilde{\Delta}$ (including the Lamb shift). As the system enters the crossover region near the lock-in time t_P , $\langle \sigma_y(\phi, t) \rangle$ continues its monotonic decay, whereas $\langle \sigma_x(\phi, t) \rangle$ develops strong interference with the bath correlation function. At the destructive-interference points, the σ_x amplitude is driven close to zero, and in their vicinity it can even fall below the amplitude of $\langle \sigma_y(\phi, t) \rangle$ [Fig. 6(c)], consistent with the behavior highlighted in the caption.

Once phase lock-in is complete, $\langle \sigma_y(\phi, t) \rangle$ is strongly suppressed relative to $\langle \sigma_x(\phi, t) \rangle$, down to a residual level of up to $O(10^{-5})$. At the same time, the σ_x phase becomes frozen, and for larger t its amplitude decays algebraically as $1/t^{s+1}$, marking the onset of phase freeze-out described in Figs. 6(e)–(f).

Taken together, these time-resolved snapshots provide the dynamical origin of the disconnected late-time structure in Fig. 5(c). The lock-in of the σ_x phase and the rapid suppression of the orthogonal quadrature imply

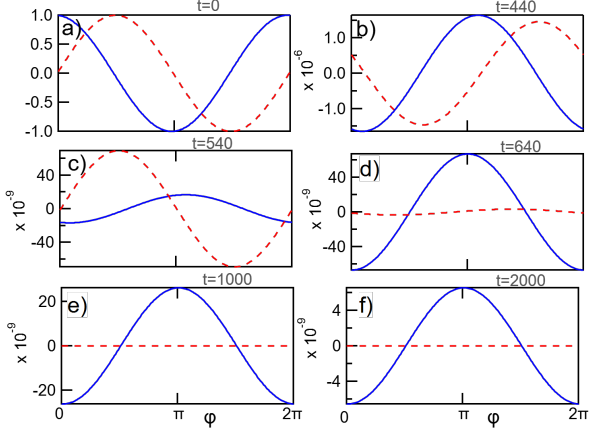


FIG. 6. **Collapse of the superposition in σ_x versus time.** The quantities $\langle \sigma_x(t, \phi) \rangle$ (blue, solid) and $\langle \sigma_y(t, \phi) \rangle$ (red, dashed) are plotted as functions of the initial azimuthal angle ϕ at six representative times t . As the magnitude of the transverse spin decays, the waves rotate with the Bohr angular velocity in (a) and (b), exhibit crossover dynamics near the lock-in time t_P in (c) and (d), and in (e) and (f) the motion freezes out and the transverse component contracts onto the selected quadrature. Note that in (c) the measurement quadrature σ_x momentarily exhibits a smaller amplitude than σ_y due to destructive interference with the bath correlation function. Also note the sign reversal in σ_x between (a) and (e,f), due to a bath-correlation phase shift of π . Parameters: $s = 1$, $\lambda^2 = 0.025$, $\omega_c = 4$, $\Delta = 1$, $\xi = 0$, $T = 0$, $\delta\phi = -0.0278$.

that, for each preparation angle ϕ , the transverse spin is ultimately funneled into a basin with definite sign of $\langle \sigma_x \rangle$. The narrow intervals in ϕ where $\langle \sigma_x(\phi, t) \rangle$ is driven through (near) zero by destructive bath interference correspond to the “interference windows” separating these basins. As a result, what appears in Fig. 6 as a crossover and projective freeze-out in time reappears in Fig. 5(c) as three disconnected late-time regions in the ϕ -dependence.

Fig. 7 shows the two-dimensional quadrature map $\langle \sigma_{x,y}(t, \phi) \rangle$ resolved in time and preparation angle. For visualization, each time slice is normalized as explained in the caption. This isolates the shape of the quadrature pattern by suppressing slow amplitude variations that would otherwise obscure the interference fringes and inter-quadrature contrast.

For $t \ll t_P$, the maxima and minima in both quadratures drift coherently in ϕ . In the crossover region, the σ_x pattern arrests and projects the initial profile at $t = 0$, up to a sign reversal fixed by the π phase shift of the bath correlation function, while σ_y continues to precess with rapidly diminishing amplitude. After lock-in, the y -quadrature is suppressed to a small residual level, whereas the selected x -quadrature retains a frozen phase and decays only algebraically, $\sim t^{-s-1}$.

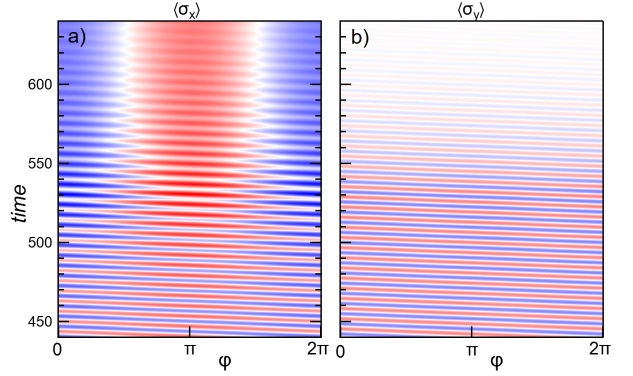


FIG. 7. **Quadrature dynamics near the lock-in scale t_P .** Panels show $\langle \sigma_x(t, \phi) \rangle$ and $\langle \sigma_y(t, \phi) \rangle$ versus time t and preparation angle ϕ , normalized by a smooth envelope fitted to the instantaneous peak-to-peak ϕ -amplitude of $\langle \sigma_x \rangle$ to remove modulation and restore quadrature contrast. The colormap is red–white–blue for $+1, 0, -1$. Near t_P the x -quadrature locks to the σ_x basis while the y -quadrature decays smoothly. At the nodes of the locked quadrature, the x -component is extinguished without reappearance, preventing zero crossings and phase slips in the full spin–boson dynamics. Parameters: $s = 1$, $\lambda^2 = 0.025$, $\omega_c = 4$, $\Delta = 1$, $\xi = 0$, $T = 0$, $\delta\phi = -0.0278$.

This provides a transparent picture of projective quantum evolution in the unbiased spin–boson model: the coupling operator σ_x uniquely selects the phase-locked quadrature, pinning the direction of the transverse spin. At this stage we do not invoke any additional detector model or imposed pointer basis: the preference for the σ_x direction follows directly from the system–bath coupling together with the algebraic long-time tail of the bath correlator captured by the reconstructed map. The amplitude of the selected component still vanishes at late times, but only through the universal long-time power law. An experimental test would be to measure the angular dependence of $t_P(\phi)$ as in Fig. 5(b).

D. Effect of the spectral exponent s

To complete the picture across bath classes, we show two representative cases away from the Ohmic point: a strongly sub-Ohmic bath ($s = 1/3$) and a deeply super-Ohmic bath ($s = 3$). As anticipated by the universal $t_P(\phi)$ trends in Fig. 6, both cases display the same qualitative sequence of exponential decay, phase lock-in, and an algebraic tail, with only quantitative shifts in the interference strength and the location of ϕ_{peak} . Since the dependence on s within each family is smooth, these two points capture the typical behavior on either side of $s = 1$.

In the sub-Ohmic case, the late-time angular response

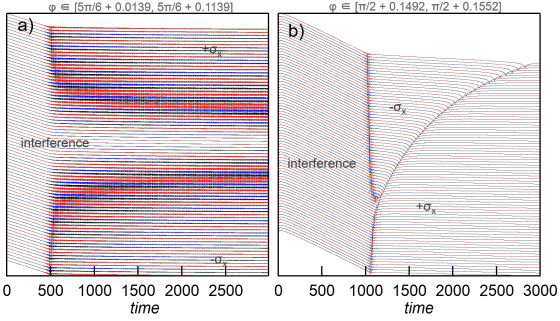


FIG. 8. **Coherence phase-locking in two bath types.** (a) For $s = 1/3$, coherence decreases slowly because the bath ‘remembers,’ creating interference that keeps the basins separate. (b) For $s = 3$ at stronger coupling, coherence drops faster and a clear bend (cusp) appears between basins. Parameters: $s = 1/3, \lambda^2 = 0.01, \delta\phi = -0.0392$ (a); $s = 3, \lambda^2 = 0.5, \delta\phi = -0.0777$ (b); $\omega_c = 4, \xi = 0, T = 0$.

remains fragmented into three disconnected ranges, with a narrow gap centered near ϕ_{peak} that separates the two σ_x basins. The gap spans $\sim 4 \times 10^{-3}\pi$, and within this window the coherence magnitude drops directly onto the algebraic bath envelope, with interference features almost entirely suppressed at its center. In other words, the bath fails to act as an efficient projector here: the transverse component is not stochastically driven into either basin but instead passes through the gap while decaying with the universal power-law tail. Free system oscillations survive throughout this interval, reaching their maximal visibility at the center of the gap, consistent with the absence of any interference with the bath correlation function.

Moving away from the gap at fixed time, one encounters a pronounced interference region before the dynamics settles again into the two outer basins, where interference is weak and free oscillations are suppressed. The basins therefore cannot be connected smoothly: any trajectory that moves from one basin to the other must traverse a strongly interfering neighborhood when leaving the first basin and another upon entering the next. The resulting ‘projector-evading’ gap thus functions as a robust separator between the phase-locked branches in the sub-Ohmic regime. Here strong bath memory does more than shift the crossover: it changes the topology of the angular response, splitting the late-time dynamics into disconnected basins.

With further increase of s the gap is strongly suppressed by $s = 1.5$ and becomes essentially invisible by $s = 3$. In this super-Ohmic range the separator collapses into a sharp cusp—the short-memory remnant of the sub-Ohmic gap—which marks the instantaneous boundary between the two basins at fixed time.

This evolution parallels the standard localization structure of the spin-boson model: for $s < 1$ strong low-frequency weight produces robust localization and max-

imal non-Markovian memory, consistent with the pronounced basin fragmentation and projector-evading gap. The Ohmic point $s = 1$ lies at the critical boundary between localized and delocalized behavior, reflected here in a residual but time-bending separator. For $s > 1$ the bath becomes effectively short-memory and localization is absent; correspondingly the gap contracts to a cusp and ultimately disappears, leaving a smooth two-basin landscape.

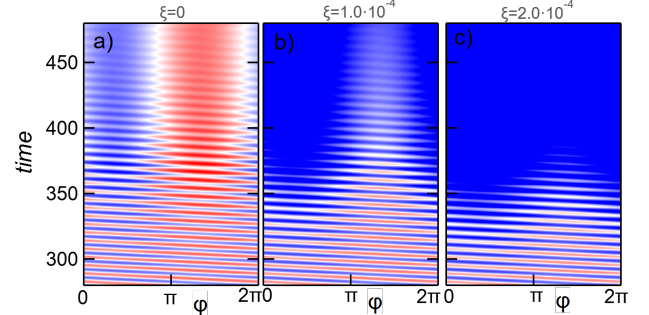


FIG. 9. **Quadrature dynamics versus bias.** Panels show $\langle \sigma_x(t, \phi) \rangle$ and versus time t and preparation angle ϕ , normalized by a smooth envelope fitted to the instantaneous peak-to-peak ϕ -amplitude of $\langle \sigma_x \rangle$ to remove modulation and restore quadrature contrast. The colormap is red-white-blue for $+1, 0, -1$. Parameters: $s = 1/3, \lambda^2 = 0.01, \omega_c = 4, \Delta = 1, T = 0, \delta\phi = -0.0278$.

E. Outlook: Finite Bias and Environment Engineering

The dynamical projection along σ_x becomes increasingly difficult to resolve once a finite bias ξ is applied. A small bias leaves the intrinsic coherence subblock in Eq. 54 only weakly perturbed, so the underlying collapse dynamics are essentially unchanged. By contrast, the population-to-coherence subblock in Eq. 52 grows rapidly with bias and quickly dominates the intrinsic coherence sector. Once the asymptotic σ_x coherence generated by this population transfer exceeds the finite lock-in amplitude, the distinct projection signature disappears: instead of collapsing onto one of the two σ_x basins, the system relaxes smoothly to a unique bias-set asymptotic coherence that is the same for all preparation angles, as shown in Fig. 9.

Increasing the coupling strength λ^2 enhances the asymptotic coherence in Eq. (50), the relaxation rate, and the effective measurement rate by a common scaling. Because these contributions grow proportionally, the crossover retains the same sensitivity to bias, and the late-time quadrature lock-in is just as fragile to bias at stronger coupling.

A more promising route is to shape the transverse noise spectrum itself. Engineered environments such as cavity

or microwave reservoirs could, in principle, be used to tailor the transverse spectrum and accelerate the collapse, but we leave such extensions to future work. However, in the present work we deliberately adopt the standard, unstructured spectral density of the original spin–boson model (the same canonical form introduced by Leggett *et al.* [6]) to demonstrate that the core SBM already contains a primitive transverse measurement channel (basis selection by dynamical phase erasure), without relying on any engineered environments.

VIII. DISCUSSION

This work addresses the long-time breakdown of time–convolutionless (TCL) descriptions in correlation-dominated regimes, where resummed time-local generators develop secular growth (“secular inflation”). We mitigate this by working at the level of the dynamical map: we decompose the evolution into a contractive Davies reference semigroup plus a non–Markovian density-matrix correlator $\mathbf{C}(t)$, and reconstruct $\mathbf{C}(t)$ with a regulated, partially resummed TCL scheme. The result is a controlled long-time reduced dynamics that remains well behaved while retaining the late-time interference physics. In the exact rotating-wave benchmark, the origin of generator spikes is transparent: interference between a Markovian pole and an algebraic tail produces near-zeros of the coherence, and ratios such as f/f convert these into inflation-like features in time-local generators. The reconstruction regulates this behavior by keeping the late-time map finite even when generator-based descriptions become ill-conditioned.

With a controlled long-time map in hand, the unbiased spin–boson model exhibits an emergent measurement consequence. Long-time bath memory and the counter-rotating sector drive late-time phase lock-in and create basins of attraction in preparation space. The reduced dynamics thereby implements a *nonselective transverse measurement primitive*: on a finite timescale t_P it irreversibly erases the relative phase between σ_x eigenspaces and suppresses the orthogonal transverse quadrature, leaving a preferred σ_x -aligned direction (with weak contrast at the times studied). This is not a QND measurement of σ_x : although the azimuthal phase becomes pinned after t_P , $\langle \sigma_x \rangle$ continues to relax (toward zero), so the σ_x populations are not conserved and repeatability is not guaranteed.

The mechanism is genuinely non–Markovian and interference-driven. It requires both long-time memory and counter-rotating processes; it disappears in the rotating-wave approximation and in the Davies weak-coupling limit, where the reduced dynamics is phase-covariant (rotation-symmetric about σ_z) and treats σ_x and σ_y equivalently. This also links the physics back to TCL breakdown: the same late-time interference that produces coherence near-zeros (and thus generator spikes) is what, once regulated at the map level, en-

ables lock-in and transverse phase erasure. Conceptually, the construction extends the Khalfin–Peres survival-amplitude picture [9, 10] from a scalar amplitude to the full reduced state via $\mathbf{C}(t)$, and it clarifies why higher-order TCL generators can amplify late-time memory effects in regime-dependent ways [13].

Numerically, the basin topology and transverse selection persist as the coupling is increased: t_P shifts and the basin splitting grows, while the qualitative structure remains stable (Appendix XII). This robustness is consistent with proximity to the Ohmic localization transition [6]. More broadly, long-time power-law tails observed in several platforms [25–28] suggest that the relevant interference regime is not model-specific. Engineered transverse environments could shorten t_P and increase the contrast of the primitive while preserving basin topology; map-level regularizations such as Choi-proximity projection [15] are complementary and may be useful at stronger coupling to enforce CPTP structure if needed.

IX. CONCLUSION

We have mitigated late-time TCL breakdown by developing a regulated, partially resummed reconstruction of the dynamical map in terms of a Davies reference flow and a non–Markovian density-matrix correlator $\mathbf{C}(t)$. The rotating-wave benchmark connects secular inflation in time-local generators to interference-induced near-zeros of the coherence and shows how the reconstruction regulates the resulting spikes at the map level. Applying the method to the unbiased spin–boson model reveals an emergent consequence of accessible long-time dynamics: late-time phase lock-in selects a transverse σ_x quadrature and yields an effective, zero-bias transverse measurement primitive (with weak contrast at the times studied), while the orthogonal σ_y is suppressed. The effect is absent in the rotating-wave approximation and in the Davies limit, identifying it as a genuinely non–Markovian interference phenomenon. The framework provides a direct bridge between long-time bath correlators, controlled dynamical-map reconstruction, and emergent measurement primitives in open quantum systems.

ACKNOWLEDGMENTS

The author thanks Jiahao Chen and Sirui Chen for valuable discussions. This work was supported by the School of Physics at the Georgia Institute of Technology through a seed grant. The author used OpenAI’s ChatGPT, an AI-based language model, to assist with editing and rephrasing the text. All scientific ideas, derivations, and conclusions are the author’s own, and the author remains fully responsible for the content.

X. VAN KAMPEN CUMULANTS AND NESTED RESUMMATIONS IN THE RWA

Roadmap. Starting from the Volterra iteration of the RWA survival amplitude, we (i) expand the solution into iterates f_n , (ii) construct the van Kampen cumulants K_{2n} via the recursion Eq. (73), (iii) isolate the secular structure using the Δ -identity Eq. (81), and (iv) show (to $O(\lambda^6)$) that the resulting cumulant series matches the nested-frequency form Eq. (92).

A. Iterated solution and cumulant recursion

Integrating both sides of Eq. (29) from 0 to t and changing the order of integration yields a Volterra integral equation of the second kind,

$$f'(t) = 1 - \frac{1}{4} \int_0^t d\tau \Gamma_\Delta(t - \tau) f'(\tau), \quad (63)$$

with the memory kernel $\Gamma_\Delta(t)$ defined in Eq. 12. To reduce notational clutter, throughout this appendix f is understood to be in the interaction picture (so we omit the prime). We use the shorthand for time ordered integrals as

$$\int \cdots \int_{\leftarrow}^t dt_{1 \dots n} = \int_0^t dt_1 \int_0^{t_1} dt_2 \cdots \int_0^{t_{n-1}} dt_n.$$

Let us write down individual terms of the series obtained by iterating Eq. (63). Defining $f(t) \equiv f_0 + f_1 + f_2 + f_3 + \dots$, we have

$$f_0 = 1, \quad (64)$$

$$f_1 = -\frac{1}{4} \int_0^t dt_1 \Gamma_\omega(t - t_1), \quad (65)$$

$$f_2 = \left(-\frac{1}{4}\right)^2 \int_{\leftarrow}^t dt_{12} \Gamma_\omega(t - t_1) \Gamma_\omega(t_1 - t_2), \quad (66)$$

$$f_3 = \left(-\frac{1}{4}\right)^3 \int_{\leftarrow}^t dt_{123} \Gamma_\omega(t - t_1) \Gamma_\omega(t_1 - t_2) \Gamma_\omega(t_2 - t_3). \quad (67)$$

For the derivatives we obtain

$$\dot{f}_0 = 0, \quad (68)$$

$$\dot{f}_1 = -\frac{1}{4} \Gamma_\omega(t), \quad (69)$$

$$\dot{f}_2 = \left(-\frac{1}{4}\right)^2 \int_0^t dt_1 \Gamma_\omega(t - t_1) \Gamma_\omega(t_1), \quad (70)$$

$$\dot{f}_3 = \left(-\frac{1}{4}\right)^3 \int_{\leftarrow}^t dt_{12} \Gamma_\omega(t - t_1) \Gamma_\omega(t_1 - t_2) \Gamma_\omega(t_2). \quad (71)$$

According to the van Kampen cumulant series, the coherence generator admits the expansion

$$\frac{\dot{f}}{f} = K_2 + K_4 + K_6 + \dots \quad (72)$$

Multiplying by f and collecting equal powers of λ^2 yields the recursive relation

$$K_{2n} = \dot{f}_n - \sum_{j=1}^{n-1} K_{2n-2j} f_j, \quad (73)$$

which is a special case of the general recursion for TCL cumulants [29]. The three lowest orders are

$$K_2 = \dot{f}_1, \quad (74)$$

$$K_4 = \dot{f}_2 - f_1 \dot{f}_1, \quad (75)$$

$$K_6 = \dot{f}_3 - f_1 \dot{f}_2 - f_2 \dot{f}_1 + f_1^2 \dot{f}_1. \quad (76)$$

Substituting the explicit iterates gives, for the RWA model,

$$K_2 = -\frac{1}{4} \Gamma_\omega(t), \quad (77)$$

$$K_4 = \frac{1}{16} \int_0^t dt_1 [\Gamma_\omega(t - t_1) - \Gamma_\omega(t)] \Gamma_\omega(t_1), \quad (78)$$

$$\begin{aligned} K_6 = & -\frac{1}{4^3} \int_{\leftarrow}^t dt_{12} \Gamma_\omega(t - t_1) \Gamma_\omega(t_1 - t_2) \Gamma_\omega(t_2) \\ & + \frac{1}{4^3} \int_0^t dt_1 \Gamma_\omega(t_1) \int_0^t dt_2 \Gamma_\omega(t - t_2) \Gamma_\omega(t_2) \\ & + \frac{1}{4^3} \Gamma_\omega(t) \iint_{\leftarrow}^t dt_{12} \Gamma_\omega(t - t_1) \Gamma_\omega(t_1 - t_2) \\ & - \frac{1}{4^3} \Gamma_\omega(t) \left[\int_0^t dt_1 \Gamma_\omega(t_1) \right]^2. \end{aligned} \quad (79)$$

B. Secular structure from the Δ identity

Define

$$\Delta(t, t_1) = \Delta \Gamma_\omega(t, t_1) \equiv \Gamma_\omega(t) - \Gamma_\omega(t_1), \quad \Gamma \equiv \Gamma_\omega(t). \quad (80)$$

This satisfies the identity [4]

$$\int \cdots \int_{\leftarrow}^t dt_{1 \dots n} \Delta(t, t - t_n) = \frac{(-i)^n}{n!} \frac{\partial^n \Gamma_\omega(t)}{\partial \omega^n}. \quad (81)$$

Thus the Δ -structure suppresses polynomial secular terms ($\sim t^n$) in the time-ordered integrals; any residual secular growth is restricted to derivatives of $\Gamma_\omega(t)$, which become dominant for algebraically decaying $C(t)$.

Using Δ , the fourth-order cumulant becomes

$$\begin{aligned} K_4 &= \frac{1}{4^2} \int_0^t dt_1 \Delta(t, t - t_1) [\Delta(t, t_1) - \Gamma] \\ &= \frac{i}{4^2} \Gamma \frac{\partial \Gamma}{\partial \omega} + \frac{1}{4^2} \int_0^t dt_1 \Delta(t, t - t_1) \Delta(t, t_1) \\ &\equiv \frac{i}{4^2} \Gamma \frac{\partial \Gamma}{\partial \omega} + \frac{1}{4^2} H_\omega(t), \end{aligned} \quad (82)$$

where we introduced

$$H_\omega(t) = \int_0^t dt_1 \Delta(t, t - t_1) \Delta(t, t_1). \quad (83)$$

Next, converting the double integrals in 79 into time-ordered form via

$$\int_0^t dt_1 X(t_1) \int_0^t dt_2 Y(t_2) = \iint_{\leftarrow}^t dt_{12} [X(t_1)Y(t_2) + X(t_2)Y(t_1)],$$

we obtain

$$K_6 = -\frac{1}{4^3} \iint_{\leftarrow}^t dt_{12} \left\{ \begin{aligned} & [\Gamma - \Delta(t, t-t_1)] [\Gamma - \Delta(t, t_1-t_2)] [\Gamma - \Delta(t, t_2)] \\ & - [\Gamma - \Delta(t, t_1)] [\Gamma - \Delta(t, t_2)] [2\Gamma - \Delta(t, t-t_2) - \Delta(t, t-t_1)] \\ & - \Gamma [\Gamma - \Delta(t, t-t_1)] [\Gamma - \Delta(t, t_1-t_2)] \\ & + 2\Gamma [\Gamma - \Delta(t, t_1)] [\Gamma - \Delta(t, t_2)] \end{aligned} \right\} \quad (84)$$

$$= K_6^\Delta + K_6^{\Delta^2} + K_6^{\Delta^3}. \quad (85)$$

The cumulant structure removes the zeroth order in Δ , so the leading nonzero contributions are linear in Δ , with Δ^2 and higher powers subleading. Using Eq. (81) and

$$\iint_{\leftarrow}^t dt_{12} \Delta(t, t-t_1) = \iint_{\leftarrow}^t dt_{12} \Delta(t, t_2),$$

the linear term yields

$$K_6^\Delta = \frac{1}{4^3} \Gamma^2 \iint_{\leftarrow}^t dt_{12} \Delta(t, t_2) = -\frac{1}{4^3} \frac{1}{2!} \Gamma^2 \frac{\partial^2 \Gamma}{\partial \omega^2}. \quad (86)$$

The quadratic contribution is

$$K_6^{\Delta^2} = -\frac{\Gamma}{4^3} \iint_{\leftarrow}^t dt_{12} \left\{ \begin{aligned} & \Delta(t, t_1-t_2) \Delta(t, t_2) - \Delta(t, t_1) \Delta(t, t-t_2) \\ & - \Delta(t, t_1) \Delta(t, t-t_1) - \Delta(t, t_2) \Delta(t, t-t_2) \end{aligned} \right\}. \quad (87)$$

Using

$$\int_0^t d\tau \Gamma_\omega(\tau) = t\Gamma_\omega(t) + i \frac{\partial \Gamma_\omega(t)}{\partial \omega}, \quad (88)$$

and

$$\int_0^t dt_1 \Gamma_\omega(t_1) \Gamma_\omega(t-t_1) = t\Gamma_\omega^2(t) + 2i\Gamma_\omega(t) \frac{\partial \Gamma_\omega(t)}{\partial \omega} + H_\omega(t), \quad (89)$$

one finds that the secular ($\sim t$) parts cancel between the two lines of Eq. (87), leaving only subleading contributions. The leading cubic term $K_6^{\Delta^3}$ remains finite and we keep it implicit.

Collecting terms gives

$$K_6 = \frac{\Gamma}{4^3} \left\{ \left[\frac{\partial \Gamma_\omega(t)}{\partial \omega} \right]^2 - i \frac{\partial H_\omega(t)}{\partial \omega} \right\} + K_6^{\Delta^3}. \quad (90)$$

C. Matching to nested frequency renormalization

Summing the cumulants to $O(\lambda^6)$ yields

$$\begin{aligned} K &= K_2 + K_4 + K_6 \\ &= -\frac{\Gamma}{4} + \frac{i}{4^2} \Gamma \frac{\partial \Gamma}{\partial \omega} + \frac{1}{4^2} H_\omega(t) - \frac{\Gamma^2}{2! 4^3} \frac{\partial^2 \Gamma}{\partial \omega^2} \\ &\quad + \frac{\Gamma}{4^3} \left[\left(\frac{\partial \Gamma_\omega(t)}{\partial \omega} \right)^2 - i \frac{\partial H_\omega(t)}{\partial \omega} \right] + K_6^{\Delta^3}. \end{aligned} \quad (91)$$

One may verify that these terms coincide with the Taylor expansion of the nested-frequency form through $O(\lambda^6)$:

$$K = -\frac{1}{4} \Gamma_{\omega - \frac{i}{4} \Gamma_{\omega - \frac{i}{4} \Gamma_\omega}} + \frac{1}{4^2} H_{\omega - \frac{i}{4} \Gamma_\omega} + K_6^{\Delta^3} + \dots \quad (92)$$

The first term exhibits frequency renormalizations nested to second order. Truncating Eq. (92) to order $O(\lambda^2)$ gives

$$K(t) \approx -\frac{1}{4} \Gamma_{u(t)}(t), \quad u(t) = \omega - \frac{i}{4} \Gamma_\omega(t),$$

which is the leading resummed generator quoted in Eq. (38).

XI. NUMERICAL DETERMINATION OF THE QUADRATURE SHIFT AND VALIDITY OF THE MAP

To extract the quadrature alignment shift, we sweep the initial angle $\phi \in [0, 2\pi]$ and evaluate the slope of $\langle \sigma_y(t, \phi) \rangle$ versus $\langle \sigma_x(t, \phi) \rangle$ at a reference time $t > t_P$, where phase lock-in is established. This slope yields $\tan \delta\phi$. For $t \gg t_P$, the rotation angle $\delta\phi$ is effectively independent of t in the phase-locked regime. Table I lists the bath exponents s and the corresponding $\delta\phi$, λ^2 and $-\phi_{\text{peak}}$ values used in this work.

To confirm that the reconstructed map is a valid quantum dynamical map, we compute the total negative eigenvalue weight of its Choi matrix. For all main-text data sets, this sum is negligibly small, indicating complete positivity to numerical precision. When nonzero, the negative weight is bounded ($\gtrsim -10^{-5}$), occurs only in the initial transient, is confined to early times, and is absent at late times and throughout the basin-locking regime. These small, short-time deviations do not show up in the observables we analyze in the basins and do not affect the physical interpretation of the dynamical map.

XII. ROBUSTNESS OF THE TRANSVERSE MEASUREMENT PRIMITIVE WITH INCREASING COUPLING STRENGTH

Increasing the Ohmic coupling by an order of magnitude leaves the late-time basin geometry essentially unchanged while shifting the lock-in scale t_P . This demonstrates that the emergent transverse measurement primitive is robust and not a weak-coupling artifact. All

TABLE I. Quadrature alignment shift $\delta\phi$, coupling constant λ^2 , and angle at maximum angle ϕ_{peak} for representative bath exponents s . The cutoff frequency is $\omega_c = 0.4$.

	$s = 0.01$	$s = \frac{1}{3}$	$s = \frac{2}{3}$	$s = 1$	$s = 1.5$	$s = 3$
$\delta\phi$	-0.3248	-0.0392	-0.1102	-0.0278	-0.0315	-0.0777
λ^2	0.005	0.01	0.02	0.025	0.05	0.5
ϕ_{peak}	0.3902	2.685	2.088	1.6292	0.8514	1.7229

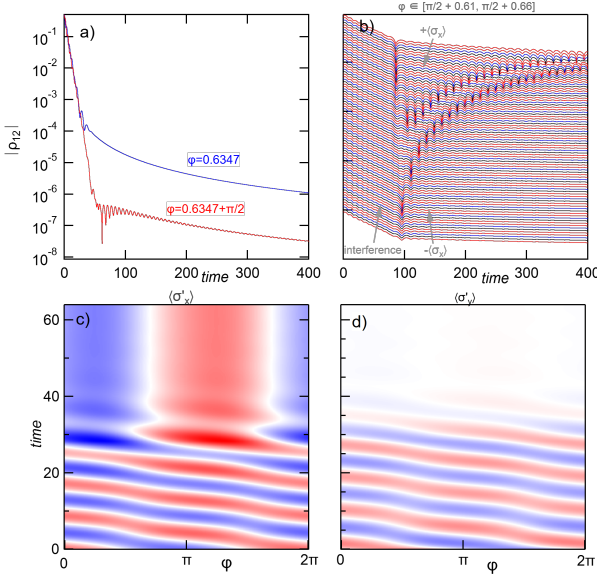


FIG. 10. **Collapse dynamics at ten-times-stronger Ohmic coupling ($\lambda^2 = 0.25$).** (a) Coherence magnitude versus time for two orthogonal transverse quadratures. (b) Late-time splitting between the two attraction basins in the locked quadrature. The asymptotic gap closely matches the weak-coupling value in Fig. 7 and is only weakly affected by the increased Ohmic strength, indicating that the underlying basin geometry is stable. (c,d) Time-resolved quadrature signals $\langle \sigma_x, y(t, \phi) \rangle$ as functions of time t and preparation angle ϕ . As in Fig. 7, each time slice is normalized by the instantaneous peak-to-peak ϕ -amplitude of $\langle \sigma_x(t, \phi) \rangle$, placing both quadratures on a fixed +1 to -1 contrast scale. The phase lock-in of the selected quadrature and the suppression and continued drift of the orthogonal quadrature follow the same pattern as at weak coupling. Parameters: $s = 1$, $\lambda^2 = 0.25$, $\omega_c = 4$, $\Delta = 1$, $\xi = 0$, $T = 0$, $\delta\phi = -0.3494$.

system parameters (Hamiltonian, bias, and state preparation) are held fixed; only the dissipation strength is changed from $\lambda^2 = 0.025$ to $\lambda^2 = 0.25$.

Comparing Fig. 5(a,b) with Fig. 10(a,b) shows that stronger dissipation increases the quadrature alignment shift (from 0.0585 to 0.6347) and enlarges the late-time basin splitting. These quantitative changes shift the angles of maximal and minimal interference with the bath correlator, while the qualitative dynamical sequence remains the same. The lock-in now occurs at $t_P \approx 30$, and near the shifted node of the locked quadrature (formerly near $\phi = \pi/2$), the coherence is strongly suppressed and exhibits the same sequence of crossovers discussed in Fig. 7. Panels 10(b-d) make this robustness explicit: the late-time basin splitting, the pinning of the selected quadrature, and the suppression of the orthogonal quadrature persist at stronger coupling.

Taken together, these observations confirm that the small locked amplitude in the weak-dissipation regime of the main text is not a perturbative artifact. The underlying mechanism—competition between the contractive Davies reference flow and the correlation-driven corrections captured by $\mathbf{C}(t)$ —remains intact as λ^2 is increased, with essentially unchanged basin topology.

At $\lambda^2 = 0.25$ the system lies within one order of magnitude of the Ohmic localization critical point identified by Leggett *et al.* [6]. The robustness observed here is consistent with approaching that threshold: as λ^2 increases further, the finite-time lock-in and phase erasure should continuously merge with the onset of permanent localization, providing a static counterpart to the correlation-driven long-time dynamics encoded in $\mathbf{C}(t)$.

-
- [1] W. H. Zurek, Physical Review D **26**, 1862 (1982).
[2] W. H. Zurek, Reviews of Modern Physics **75**, 715 (2003).
[3] J. P. Paz and W. H. Zurek, Physical Review Letters **82**, 5181 (1999).
[4] L. Lampert, S. Gadamsetty, S. Chaudhary, Y. Pei, J. Chen, E. Crowder, and D. Davidović, Physical Review A **111**, 042214 (2025).
[5] C. Blumenfeld, Modifying the time-convolutionless master equation via the moore-penrose pseudoinverse (2025), arXiv:2511.02556 [quant-ph].
[6] A. J. Leggett, S. Chakravarty, A. T. Dorsey, M. P. A. Fisher, A. Garg, and W. Zwerger, Rev. Mod. Phys. **59**, 1 (1987).
[7] U. Weiss, *Quantum Dissipative Systems*, 4th ed. (WORLD SCIENTIFIC, 2012) <https://www.worldscientific.com/doi/pdf/10.1142/8334>.
[8] A. A. Clerk, M. H. Devoret, S. M. Girvin, F. Marquardt, and R. J. Schoelkopf, Reviews of Modern Physics **82**,

- 1155 (2010).
- [9] L. A. Khalfin, Sov. Phys. JETP **6**, 1053 (1958).
- [10] A. Peres, Annals of Physics **129**, 33 (1980).
- [11] E. Torrontegui, J. G. Muga, J. Martorell, and D. W. L. Sprung, in *Advances in Quantum Chemistry*, Vol. 60 (Elsevier, 2010) pp. 485–536.
- [12] S. M. Wang, W. Nazarewicz, A. Volya, and Y. G. Ma, Phys. Rev. Res. **5**, 023183 (2023).
- [13] P. Kumar, K. P. Athulya, and S. Ghosh, Asymptotic tcl4 generator for the spin-boson model: Analytical derivation and benchmarking (2025), arXiv:2506.17009 [quant-ph].
- [14] G. Kaplanek and C. Burgess, Journal of High Energy Physics **2020**, 1 (2020).
- [15] A. D'Abbruzzo, D. Farina, and V. Giovannetti, Phys. Rev. X **14**, 031010 (2024).
- [16] H.-P. Breuer and F. Petruccione, *The theory of open quantum systems* (Oxford University Press, Oxford, 2007).
- [17] E. B. Davies, Comm. Math. Phys. **39**, 91 (1974).
- [18] W. De Roeck and A. Kupiainen, in *Annales Henri Poincaré*, Vol. 14 (Springer, 2013) pp. 253–311.
- [19] M. Merkli, Quantum **6**, 615 (2022).
- [20] B. Vacchini and H.-P. Breuer, Physical Review A—Atomic, Molecular, and Optical Physics **81**, 042103 (2010).
- [21] W.-M. Zhang, P.-Y. Lo, H.-N. Xiong, M. W.-Y. Tu, and F. Nori, Physical review letters **109**, 170402 (2012).
- [22] E. Crowder, L. Lampert, G. Manchanda, B. Shoffeitt, S. Gadamssetty, Y. Pei, S. Chaudhary, and D. Davidović, Phys. Rev. A **109**, 052205 (2024).
- [23] P. Kumar, K. Athulya, and S. Ghosh, arXiv preprint arXiv:2411.08869 (2024).
- [24] A. Trushechkin, M. Merkli, J. Cresser, and J. Anders, AVS Quantum Science **4** (2022).
- [25] C. Rothe, S. I. Hintschich, and A. P. Monkman, Phys. Rev. Lett. **96**, 163601 (2006).
- [26] A. Crespi, F. V. Pepe, P. Facchi, F. Sciarrino, P. Mataloni, H. Nakazato, S. Pascazio, and R. Osellame, Phys. Rev. Lett. **122**, 130401 (2019).
- [27] I. A. Merkulov, A. L. Efros, and M. Rosen, Phys. Rev. B **65**, 205309 (2002).
- [28] F. H. L. Koppens, K. C. Nowack, and L. M. K. Vandersypen, Phys. Rev. Lett. **100**, 236802 (2008).
- [29] K. Nestmann and C. Timm, Time-convolutionless master equation: Perturbative expansions to arbitrary order and application to quantum dots (2019), arXiv:1903.05132 [cond-mat.mes-hall].